Cement & Concrete Composites 37 (2013) 215–221

Contents lists available at SciVerse ScienceDirect

Cement & Concrete Composites

journal homepage: www.elsevier.com/locate/cemconcomp

Nanoscale mechanical properties of concrete containing blast furnace slag and fly ash before and after thermal damage

Vahid Zanjani Zadeh, Christopher P. Bobko *

North Carolina State University, Civil, Construction and Environmental Engineering, Campus Box 7098, Raleigh, NC 27695, USA

ARTICLE INFO

Article history:
Received 19 March 2012
Received in revised form 14 September 2012
Accepted 20 September 2012
Available online 17 October 2012

Keywords:
Fly ash
Blast furnace slag
Nanoindentation
Microstructure
Fire damage
Hydration products

ABSTRACT

Portland cement blended with waste products such as blast furnace slag and fly ash are frequently used to create more sustainable concrete, but their nanoscale mechanical behavior, particularly after thermal damage, has not been well-studied. Here, nanoindentation experiments confirm that concrete produced with blended cements contains hydration products with nearly identical nanoscale mechanical properties to the hydration products found in concretes produced with ordinary Portland cement. The volume fractions of the hydration products, particularly calcium-silicate-hydrate (C-S-H) phases, are formed in different proportions with the addition of fly ash and blast furnace slag. After exposure to fire damage, the nanoscale behavior of concretes produced with fly ash and slag also matches the nanoscale behavior of conventional concretes. This suggests that any macroscopic differences between fire damage behavior of blended cement concrete and ordinary Portland cement concrete must have origins in a larger length scale.

© 2012 Elsevier Ltd. All rights reserved.

1. Introduction

Blast furnace slag and fly ash have been used extensively as a successful replacement material for Portland cement in concrete materials to improve durability, produce high strength and high performance concrete, and bring environmental and economic benefits such as resource conservation and energy savings [1,2]. Standards and practices for using concrete materials are based on years of experiments, research, and experience with conventional concretes, but significantly less information is available for concretes with replacement materials. Therefore, additional information about nanoscale mechanical properties of concrete with slag and fly ash is useful. If nanoscale structure and behavior is similar for conventional and more sustainable concrete mixes, we may have more confidence in applying conventional standards and practices to more sustainable concretes. Assessment of behavior after events that may damage concrete is of special concern. For example, as part of a structure, concrete produced with supplementary materials such as slag and fly ash may be exposed to fire in its lifetime. Therefore, assessing the mechanical behavior of the concrete after exposure to high temperature is critically important. In the present study, nanoscale performance of concrete containing slag and fly ash, both intact and after damage by exposure to elevated temperature, was investigated using a statistical nanoindentation technique in the submicron length scale.

1.1. Nanoscale mechanical properties of C-S-H

It is well established that calcium silicate hydrate (C-S-H) and portlandite (CH) are two main hydration products of calcium silicate based cements. Recent studies by Ulm and coworkers have illustrated that there are three types of C-S-H (LD C-S-H, HD C-S-H, UHD C-S-H) in hardened cement paste [3–8]. UHD C-S-H is believed to be a C-S-H/CH nanocomposite [7] rather than a pure C-S-H phase. Together with other research by Jennings [9,10], a useful model suggests that LD C-S-H and HD C-S-H are composed mainly of elementary particles with different nanoscale porosity, while the UHD C-S-H is a nanocomposite composed of the same elementary C-S-H particles and nanoscale CH crystals [7]. The average nanoscale material responses (e.g. indentation modulus and indentation hardness) for each of these three C-S-H phases are virtually the same for all Portland cement pastes tested to date [3–8]. From a cement chemistry perspective, the identified C-S-H phases may not be purely C-S-H, but could also be representative of composite action with intermixed nanoscale crystals, produced in preferential microstructures [7]. Still, the LD, HD, and UHD C-S-H model is a useful one and highlights the importance of porosity and packing density in the primary binding phase of Portland cement concrete.

The hydration of Portland cement blended with slag or fly ash is more complex than that of pure Portland cement. In concrete

* Corresponding author. Tel.: +1 919 515 0481.
E-mail addresses: vzanjan@ncsu.edu (V. Zanjani Zadeh), chris_bobko@ncsu.edu (C.P. Bobko).

0958-9465/$ - see front matter © 2012 Elsevier Ltd. All rights reserved.
http://dx.doi.org/10.1016/j.cemconcomp.2012.09.003

incorporating fly ash or slag, calcium hydroxide reacts with slag and fly ash to form calcium-silicate-hydrates [2], and in pastes with slag, the slag also hydrates simultaneously and reacts with other products [11]. XRD studies show that the main hydration products of Portland cement blended with slag is essentially similar to those formed by hydration of pure Portland cements [12], although calcium/silica ratios may be different [13,14]. Pore volumes in cements blended with fly ash or slag tend to be greater than that of similar paste made from pure Portland cement. However, they have finer pore distributions than normal concrete [11,15,16]. In later ages, the pores in hardened slag-cement pastes are more discontinuous than those in Portland cement pastes [17]. Vandamme has performed indentation on cements with silica fume and a calcareous filler [18] and Sorrelli et al. have reported on an Ultra-High Performance Concrete that includes silica fume [8]. These studies have also suggested that the main hydration products have similar products to those formed by pure Portland cement. Sakulich and Li [19] presented limited results on engineered cementitious composites with high fiber contents but did not perform enough tests to distinguish individual phases in cement paste. No other nanoindentation results on blended cements with fly ash or slag are currently available in the literature.

1.2. Fire damage in cement paste and concrete

Generally, concrete is considered to have inherently fire-resistant properties owing to its low thermal conductivity and high specific heat; however, it undergoes changes in its chemical composition and physical properties when it is exposed to elevated temperature [20,21]. The most important effects of elevated temperature on concrete are: dehydration of cement paste, porosity increase, strength loss, alteration of pore pressure, modification of moisture content, thermal expansion, thermal creep, and spalling due to excessive pore pressure [22,23].

Many researchers have studied the resistance of concrete, with and without supplementary cementitious materials, to elevated temperatures [24–27]. Dehydration or loss of the non-evaporable water or water of hydration begins to take place when the temperature reaches 250 °C. Degradation becomes more pronounced between 200 °C and 250 °C. At 300 °C strength reduction is expected to be in the range of 15–40%, whereas at 550 °C and 700 °C reduction in compressive strength would typically range from 55% to 70% of its original value [28–31].

The resistance of concrete incorporating ultra-fine cementing materials such as metakaolin and silica fume is typically reported to be lower than normal concrete, while other supplementary cementitious materials (SCMs), including fly ash and slag, may have a similar or better response to high temperatures compared to normal concrete [13,32–43]. Overall, there is a tradeoff between competing phenomena when SCMs are added to concrete. Refinement of pores or densification of the microstructure, typically associated with addition of SCMs, leads to a greater pressure build up of water vapor when concrete is heated. This in turn leads to cracking and potentially to explosive spalling. On the other hand, reduction of CH during secondary reactions with SCMs can be advantageous because CH crystals are often an initial point of cracking during heating, and SCMs make the microstructure more homogeneous.

Overall changes in mechanical properties due to elevated temperature can be tested by conventional methods. However, some phenomena that are interlinked directly with the microstructure can be disclosed exclusively by small scale methods like nanoindentation or SEM image analysis. A few researchers have used image analysis to detect morphological alteration and microcracks of thermally damaged concrete [20,31,44]. A recent study has evaluated changes in crack density for blended cements exposed to temperature [45]. DeJong and Ulm investigated the degradation of cement paste exposed to elevated temperatures at the nanoscale using the statistical nanoindentation technique [4]. In summary, research suggests that the deterioration of strength and stiffness of cement paste materials with temperature is a result of dehydration of the main hydration products (CH and C-S-H), and of formation of cracks at a larger scale. Changes in the C-S-H phases are observable by nanoindentation, and these changes are the damage mechanism investigated in this study.

2. Experimental program

2.1. Materials

Three concrete mixtures with different percentages of fly ash and slag were produced for another study to assess crack density and elastic properties of fire-damaged sustainable concrete [45]. The total Portland cement (Type II) in the mixture was replaced by 20% fly ash (Class F), 60% fly ash (Class F), or 60% slag cement (grade 100) by weight. 20% fly ash replacement and 60% slag cement replacement are quantities often found in commercial construction, while 60% fly ash is quite high but could be considered for enhanced sustainability. The water to binder ratio for all three samples was 0.45. The composition of mixtures is shown in Table 1.

Standard tests were performed on companion cylinders and results from these tests, along with more details about the samples and their preparation, are reported by McCoy [45]. Curing conditions are particularly relevant to this study. Fourteen 10.16 cm × 20.32 cm cylinders were fabricated for each of the three mixtures. Initial curing took place in the sealed cylinders for 48 h, and after samples were removed from the molds, they were cured in accordance with ASTM C31-08 for 36 days. Two disks, approximately 2.5 cm thick, were cut from the middle of the cylinders and the disks were cured for 20 more days. From each mixture, one disk was air dried for 3 weeks, exposed to 300 °C heat, submersed in a water bath for 7 days for crack density testing and then removed to an air-dried state again. The nanoindentation tests were performed on samples from the air-dried disks months later.

For nanoindentation, three small scale samples were taken from disk specimens, and trimmed using a diamond saw in low speed. The dimensions of the samples were about 2.5 cm × 2.5 cm × 2.5 cm. Special attention was paid in preparation of the samples, particularly in polishing and preparation of the sample surfaces, since it could affect the results by introducing new length scale into the analysis. In order to reach appropriate surface roughness, according to Ref. [46] the samples were cut by diamond saw, and then were ground with decreasingly rough abrasive papers to have almost smooth and flat surfaces in all faces. Next, the upper surfaces were polished with 1 μm alumina pastes and propylene glycol on a Tex Met P pad for one to two hours. The surfaces were observed under a reflected light microscope frequently to check the effectiveness of the polishing. The polishing continued until desired surface smoothness was achieved [46]. In order to check the surface roughness, Atomic Force Microscopy (AFM) was used to assess the topography of the sample surfaces. Root mean square

Table 1
Mixture compositions (in kg/m^3).

	20% fly ash	60% fly ash	60% slag
Portland cement (Type II)	296	148	148
Fly ash (Class F)	74	222	–
Slag cement (grade 100)	–	–	222
Sand (natural, C33)	644	584	653
Stone (#67 C33)	1068	1068	1068
Water	168	168	168

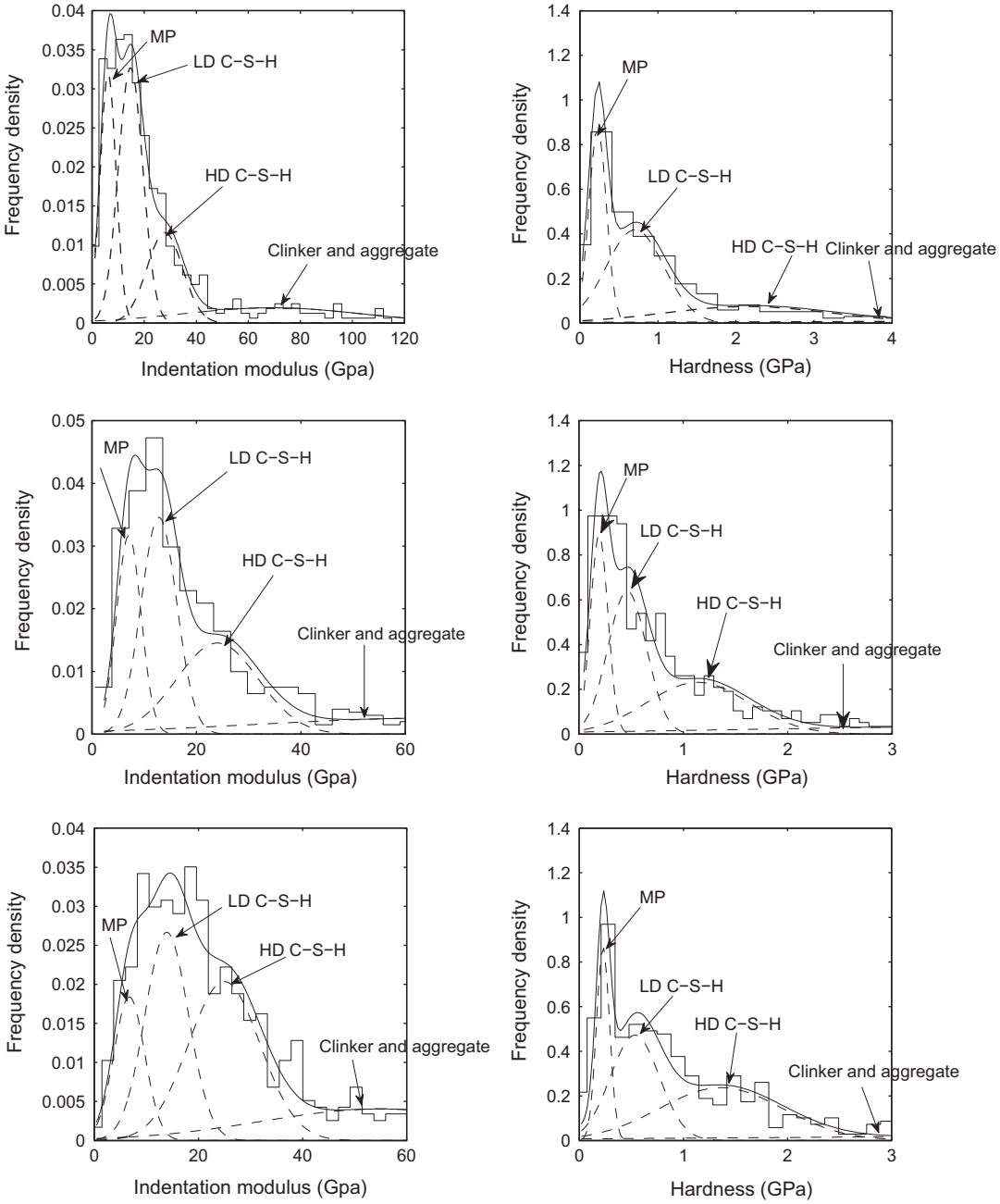

Fig. 1. Probability distribution graphs of indentation modulus and hardness for undamaged samples with 20% and 60% fly ash and 60% slag. From left to right (increasing indentation modulus and hardness) the first peak is macroporosity, the second peak is LD C-S-H, and the third peak is HD C-S-H.

(RMS) [46] roughness measurement of the samples were 4.53 nm, 4.33 nm, and 6.19 nm for undamaged samples with 20% fly ash, 60% fly ash, and 60% slag, and 8.49 nm, 8.44 nm, and 38.5 nm for damaged samples with 20% fly ash, 60% fly ash, and 60% slag respectively. The images were obtained on 40×40 μm areas and a Gaussian filter was applied to filter out spatial wavelength than 8 μm which is out of proportion of characteristic size of the nanoindentation. Since average indentation depth was five times greater than the RMS roughness, roughness of the sample surfaces was acceptable following the criteria proposed by Miller et al. [46].

2.2. Grid nanoindentation tests

Grid nanoindentation is an experimental technique for obtaining quantitative data on heterogeneous materials, typically in submicron length scale, by following procedures presented by Ulm and co-workers [3–6]. Large grids of nanoindentation measurements are performed and a statistical analysis is made to identify individual phase properties and volume fractions. Trtik et al. [47,48] have questioned the application of grid indentation technique in cementitious materials. They argued that it is impossible to obtain appropriate surface roughnesses less than 1 μm, and that in cement paste, there is no homogenous region with characteristic size larger than 2 μm, the volume sensed beneath an indenter for typical indentation testing on cement. They have also called early statistical deconvolution methods into question. They believe these conditions contradict the assumptions in grid nanoindentation analysis and prevent accurate identification of material phases. Ulm et al. [49] subsequently discussed flaws in Trtik et al.'s analysis, questioning their modeling methods and

Table 2
Indentation modulus, hardness and volume fraction of hydration products in undamaged concrete.

	LD C-S-H	HD C-S-H	UHD C-S-H or CH
Indentation modulus, M			
OPC (w/c = 0.4), Vandamme et al. [6]	22.5 ± 5.0	30.4 ± 2.9	40.9 ± 7.7
OPC (w/c = 0.5), DeJong and Ulm [4]	19.1 ± 5.0	32.2 ± 3.0	39.7 ± 4.5
OPC with 21% silica fume (w/b = 0.4), Vandamme [18]	23.64 ± 4.07	30.59 ± 2.87	42.18 ± 5.87
OPC with 20% fly ash (w/b = 0.45)	18.72 ± 7.1	35.00 ± 6.5	–
OPC with 60% fly ash (w/b = 0.45)	15.82 ± 5.12	32.88 ± 8.0	–
OPC with 60% slag (w/b = 0.45)	21.63 ± 6.68	33.66 ± 7.59	–
Indentation hardness, H			
OPC (w/c = 0.4), Vandamme et al. [6]	0.61 ± 0.17	0.92 ± 0.1	1.46 ± 0.45
OPC (w/c = 0.5), DeJong and Ulm [4]	0.66 ± 0.29	1.29 ± 0.11	1.65 ± 0.17
OPC with 21% silica fume (w/b = 0.4), Vandamme [18]	0.62 ± 0.13	0.91 ± 0.11	1.42 ± 0.40
OPC with 20% fly ash (w/b = 0.45)	0.93 ± 0.38	3.68 ± 1.98	–
OPC with 60% fly ash (w/b = 0.45)	0.87 ± 0.34	3.14 ± 0.89	–
OPC with 60% slag (w/b = 0.45)	0.97 ± 0.41	2.55 ± 1.13	–
Volume fraction, f			
OPC (w/c = 0.4), Vandamme et al. [6]	0.57	0.21	0.22
OPC (w/c = 0.5), DeJong and Ulm [4]	0.77	0.12	0.11
OPC with 21% silica fume (w/b = 0.4), Vandamme [18]	0.60	0.21	0.19
OPC with 20% fly ash (w/b = 0.45)	0.65	0.35	–
OPC with 60% fly ash (w/b = 0.45)	0.57	0.43	–
OPC with 60% slag (w/b = 0.45)	0.65	0.35	–

conclusions. With respect to claims about statistical analysis, Trtik et al. discuss an early generation of statistical deconvolution tools, while current methods, including those used in research presented here, are more robust. Finally, Chen et al.'s [7] work combines nanoindentation testing and Energy Dispersive X-ray analysis in a scanning electron microscope applied to cement paste. Their results provide support for the possibility of nanoscale crystalline phases within C-S-H phases, while also observing distinct groupings of mechanical properties, similar to earlier work reported by Ulm and co-workers.

In this study, six sets of grid nanoindentation tests were carried out on the samples: three control samples and three which were exposed to high temperature. Several arbitrarily chosen areas were selected, and were indented by means of massive grid indentation in order to receive a large statistical set of data from all material phases. Since cement matrix properties were of interest, indentation locations were chosen not to contain large grains of aggregate or large pores. Each location was covered by a rectangular grid of indents with 10 μm spacing in both directions. Roughly 400 indents were performed on each location.

Indentation loading proceeds with a linear loading up to 2 mN at a constant rate of 4 mN/min, a holding period at the peak for 5 s, and a linear unloading with same rate as loading, following prior research on cement paste [3–7]. This loading gives an average maximum indentation depth of ~200 nm which is sufficient to assess the mechanical behavior of hydrated material phases including LD and HD C-S-H. Indentation modulus and hardness were extracted from the load–deformation history of each individual indent using the Oliver and Pharr [50] method:

$$H = \frac{P_{\max}}{A_c} \quad M = \frac{\sqrt{\pi}}{2}\frac{S}{\sqrt{A_c}} \tag{1}$$

where P_{max}, A_c, and S represent the peak indentation load, the associated projected contact area and the slope of the upper portion of the unloading curve respectively.

Statistical analysis of data can then provide reliable mechanical measurements for individual phases and identify relative volume fractions and spatial distributions of these phases in complex heterogeneous composites. Assume a heterogeneous material that is composed of $j = 1\ldots m$ phases, and $i = 1\ldots N$ indentation tests have been done on the material. The properties of each phase are identified as:

$$f_j = \frac{N_j}{N} \quad \sum_{j=1}^{m} N_j = N \tag{2}$$

$$\mu_j^{\alpha} = \frac{1}{N_j}\sum_{n=1}^{N_j} x_i^{\alpha} \quad (\sigma_j^{\alpha})^2 = \frac{1}{N_j - 1}\sum_{n=1}^{N_j}(x_i^{\alpha} - \mu_j^{\alpha})^2 \tag{3}$$

where x_i^{α} represents one such mechanical property ($\alpha = M, H$) from a single indentation test, and f_j, μ_j^{α} and σ_j^{α} stand for volume fraction, mean and standard deviation of mechanically distinct phases respectively. Also N_j denotes the number of indentations on material phase j and N is the total number of indentation tests. The core purpose of any deconvolution method is to estimate five unknowns, $\{\mu_j^M, \sigma_j^M, \mu_j^H, \sigma_j^H, f_j\}$ per phase j.

Early deconvolution methods for grid indentation data sought the unknown values using a sum of Gaussian distributions in an experimental probability density function (PDF) [5]. In this method, probability density functions are based on uncorrelated outcomes (M, H) which are linked only by volume fraction, but M and H are the output of a single experiment and are expected to be correlated. To overcome this problem, an alternative method of analyzing grid indentation results using finite Gaussian mixture models has recently been introduced [51]. In this model an expectation–maximization (EM) algorithm, an iterative method, is applied to estimate the maximum likelihood (ML) function which is used to estimate parameters and the most appropriate number of observed phases. In this study, the estimation of indentation parameters using an EM algorithm and ML function was implemented by a non-commercial program (EMMIX) developed by McLachlan et al. [52,53].

3. Results

3.1. Undamaged concrete with blended cements

Distinguishable sets of nanoindentation results corresponding to material phases in hardened concrete were separated by the Gaussian mixture model deconvolution method. For a more intuitive presentation of the results, probability density distributions of indentation modulus and hardness are shown in Fig. 1. Identified phases include LD C-S-H, HD C-S-H, and zones dominated by macroporosity (capillary porosity), which is present because the

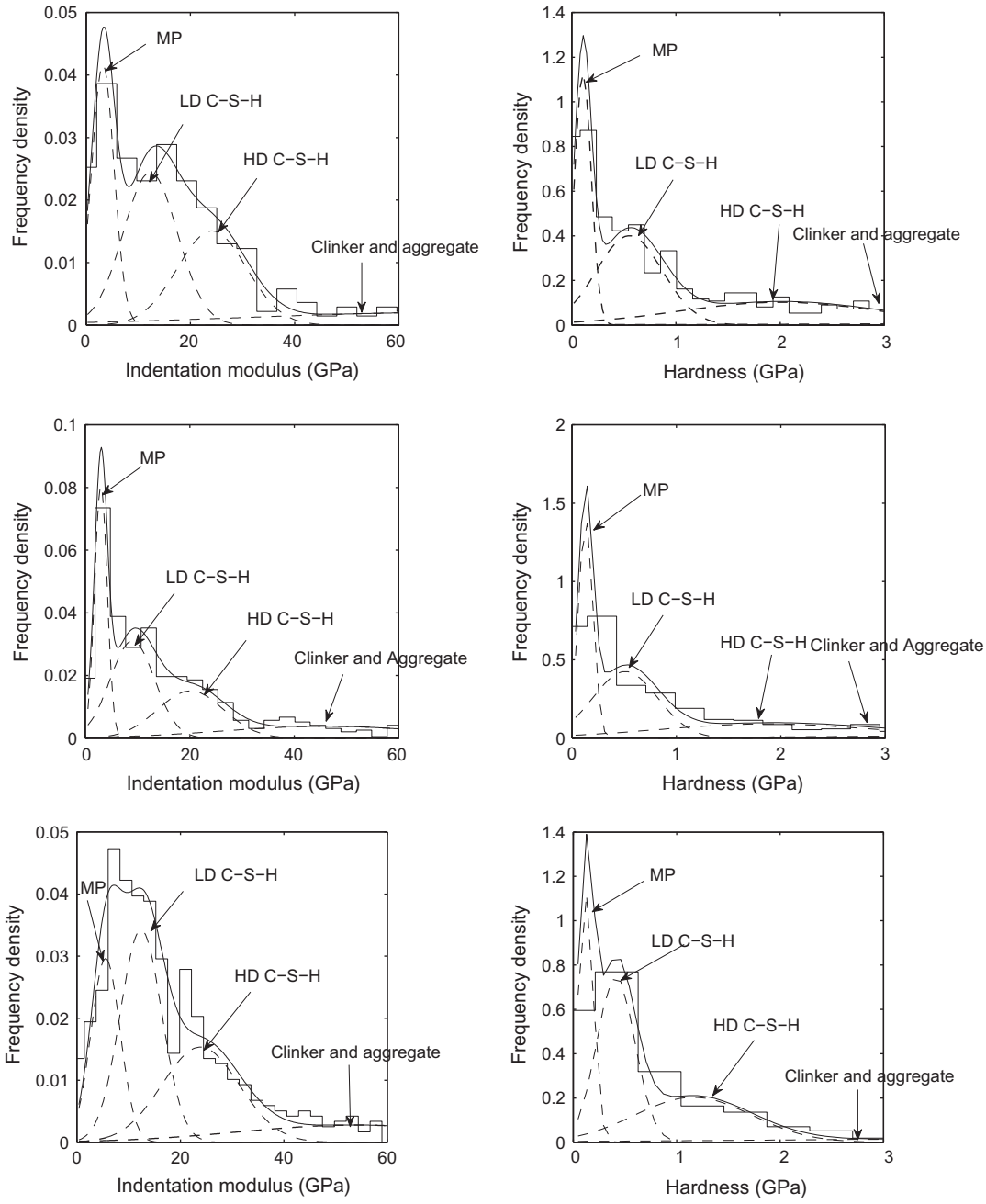

Fig. 2. Probability distribution graphs of indentation modulus and hardness for the damaged samples with 20% and 60% fly ash and 60% slag. From left to right (increasing indentation modulus and hardness) the first peak is macroporosity, the second peak is LD C-S-H, and the third peak is HD C-S-H.

w/b ratio is above the stoichiometric limit. The indentation modulus, hardness, and volume fractions of C-S-H phases of undamaged samples are displayed in Table 2. The volume fractions are normalized to the total volume fraction of C-S-H phases since zones for grid indentation were chosen to avoid areas of aggregate.

The average values for indentation moduli of the C-S-H phases are similar to those quoted in the literature [4,6,7], also displayed in Table 2. The indentation hardness is higher than expected, especially for HD C-S-H; the reason for this discrepancy is unclear but must be a secondary effect of the fly ash and slag. Note that in the blended cements, a UHD C-S-H phase is completely absent in the indentation results, and that the volume fractions of LD and HD C-S-H phases are affected by the presence of fly ash or slag because portlandite reacts with fly ash and slag and yields more C-S-H. This additional C-S-H appears to form as HD C-S-H by comparison of volume fractions of C-S-H phases for the different samples. Average maximum indentation depths were 285.5, 367.8, and 374.8 nm for samples with 20%, 60% fly ash, and 60% slag respectively.

3.2. High temperature damaged concrete

Probability density distributions of indentation modulus and hardness for the samples damaged by exposure to 300 °C are shown in Fig. 2, and deconvolution results for these samples are listed in Table 3. The same hydrated phases found in the control samples were found in the concrete samples exposed to heat. Also, the volume fraction for all the phases was almost the same before

Table 3
Indentation modulus, hardness and volume fraction of hydration products in damaged samples.

	LD C-S-H	HD C-S-H	UHD C-S-H or CH
Indentation modulus, M			
OPC (w/c = 0.5), DeJong and Ulm [4]	14.2 ± 5.4	25.7 ± 6.1	40.0 ± 8.2
OPC with 20% fly ash (w/b = 0.45)	12.31 ± 5.14	25.73 ± 12.74	–
OPC with 60% fly ash (w/b = 0.45)	12.82 ± 5.54	30.08 ± 13.45	–
OPC with 60% slag (w/b = 0.45)	13.84 ± 5.22	27.98 ± 11.38	–
Indentation hardness, H			
OPC (w/c = 0.5), DeJong and Ulm [4]	0.55 ± 0.27	1.26 ± 0.24	1.92 ± 0.22
OPC with 20% fly ash (w/b = 0.45)	0.64 ± 0.34	2.31 ± 1.26	–
OPC with 60% fly ash (w/b = 0.45)	0.57 ± 0.38	2.21 ± 1.42	–
OPC with 60% slag (w/b = 0.45)	0.46 ± 0.22	1.59 ± 0.83	–
Volume fraction, f			
OPC (w/c = 0.5), DeJong and Ulm [4]	0.76	0.24	Unknown
OPC with 20% fly ash (w/b = 0.45)	0.61	0.39	–
OPC with 60% fly ash (w/b = 0.45)	0.53	0.47	–
OPC with 60% slag (w/b = 0.45)	0.60	0.40	–

and after exposure to high temperature. However, high temperature had a considerable effect on mean values of hardness and indentation modulus of the phases. All the mean values of damaged samples were lower than those in the control samples, although indentation hardness was still somewhat higher than expected in our samples with fly ash or slag. For ordinary cement pastes, Dejong and Ulm [4] also reported a decline in indentation parameters for normal cement paste after exposing to high temperature. Their data from 300 °C is also shown in Table 3, although DeJong and Ulm did not report volume fraction values for CH or UHD C-S-H phases. The average maximum indentation depths were 310.4 nm, 290.2 nm, and 352.9 nm for damaged samples with 20%, 60% fly ash, and 60% slag respectively.

4. Discussion

The nanoindentation results demonstrate that nanoscale elastic properties of hydration products are the same or similar for conventional and blended cements, under normal conditions or after high temperature exposure. These results are similar to those found by Vandamme [18] for undamaged cement pastes with silica fume with a wide variety of different water/cement ratios. From a mechanical perspective, the hydration products in conventional cements and blended cements cannot be distinguished except by some differences in indentation hardness, confirming observations from XRD measurements [11].

Volume fractions of hydration products do vary with cement replacement. Vandamme et al. [6] have shown that the volume fractions of hydration products are highly dependent on the w/c ratio of the cement paste. It could be argued that in our blended cement samples, the water/cement ratio is more relevant than the water/binder ratio, but the nanoindentation results suggest that the water/binder ratio is most appropriate. As shown in Tables 2 and 3, the volume fraction of LD C-S-H for the studied blended concretes with w/b ratio of 0.453 falls in between reported values for w/c ratios of 0.4 and 0.5, and is fairly consistent between all three samples. Water/cement ratios of 0.56 for the 20% fly ash sample and 1.13 for the 60% fly ash and 60% slag samples would be higher than those for any other nanoindentation experiments available in the literature. Since these ratios are well above the stoichiometric limit, it is reasonable to expect only small deviation in volume fractions of C-S-H phases from those in samples with w/c ratios near 0.5.

Tables 2 and 3 also show that in samples with blended cements, no UHD C-S-H was found, and instead the remaining hydration products consist of a higher fraction of HD C-S-H phases compared to ordinary Portland cements with similar water/cement ratios. In cements incorporating fly ash and slag, calcium hydroxide reacts with slag and fly ash [11], thereby limiting the presence of UHD C-S-H (C-S-H/CH nanocomposites) or any other form of CH, at least after the secondary reactions begin. Similar results were found by Vandamme [18] for silica fume, although his results still suggested the presence of a UHD C-S-H/CH nanocomposite with bound CH that did not participate in a secondary reaction. The w/b ratio used in this study, however, was higher than in Vandamme's work. This could account for the absence of UHD C-S-H in our samples, because high w/c ratios inhibit the production of UHD C-S-H [6].

In contrast to some macroscopic observations that concretes with blended cements are more sensitive to high temperatures than conventional concretes, our data demonstrate that the nanoscale degradation of mechanical properties in blended cements is similar to that for conventional concretes. This suggests that macroscopic differences between damage of blended cements and conventional cements must arise from some microstructural feature at a scale larger than the scale of C-S-H hydration products.

5. Conclusions

1. The nanoscale elastic behavior of C-S-H phases in cement paste formed by ordinary Portland cement and cements blended with fly ash and blast furnace slag are virtually identical. Similar results were found for undamaged cements with silica fume. Some difference in indentation hardness was observed. Even if the chemical composition of the hydration products from blended cements is slightly different, their mechanical behavior may be modeled as indistinguishable from hydration products of ordinary Portland cement.
2. In blended cements, the secondary reaction consumes portlandite, and therefore limits the presence of UHD C-S-H, a nanocomposite phase containing C-S-H and CH [7] found in ordinary cement pastes.
3. After exposure to temperatures associated with fire damage, hydration products in the blended cements experienced degradation of mechanical properties following a similar trend as ordinary Portland cement.
4. The water/binder ratios tested in this study were above the stoichiometric limit. Further research to assess the effects of blended cements on volume fractions of C-S-H phases in mixes with low water/binder or water/cement ratios would be valuable for building or validating models of hydration and evolution of mechanical properties across a wide range of possible mix designs.

Acknowledgements

The authors are grateful to Dr. Michael Leming and Brad McCoy for providing samples and to Dr. Leming for helpful discussions.

References

[1] Odler I. Special inorganic cements, modern concrete technology series. New York: E & FN Spon; 2000.
[2] Metha PK, Monteiro JMP. Concrete: microstructure, properties and materials. New York: McGraw-Hill; 2006.
[3] Constantinides G, Ulm FJ. The nanogranular nature of C-S-H. J Mech Phys Solids 2007;55(1):64–90.
[4] Dejong MJ, Ulm FJ. The nanogranular behavior of C-S-H at elevated temperatures (up to 700 °C). Cem Concr Res 2007;37(1):1–12.
[5] Ulm FJ, Vandamme V, Bobko C, Ortega JA, Tai K, Ortiz C. Statistical indentation techniques for hydrated nanocomposites: concrete, bone, and shale. J Am Ceram Soc 2007;90(9):2677–92.
[6] Vandamme M, Ulm FJ, Fonollosa P. Nanogranular packing of C-S-H at substochiometric conditions. Cem Concr Res 2010;40(1):14–26.
[7] Chen J, Sorrelli L, Vandamme M, Ulm FJ, Chavillard G. A coupled nanoindentation/SEM–EDS study on low water/cement ratio Portland cement paste: evidence for C-S-H/$Ca(OH)_2$ nanocomposites. J Am Ceram Soc 2010;93(5):1484–93.
[8] Sorelli L, Constantinides G, Ulm FJ, Toutlemonde F. The nano-mechanical signature of ultra high performance concrete by statistical nanoindentation techniques. Cem Concr Res 2008;38(12):1447–56.
[9] Jennings HM. A model for the microstructure of calcium silicate hydrate in cement paste. Cem Concr Res 2000;30(1):101–16.
[10] Jennings HM. Refinements to colloid model of C-S-H in cement: CM-II. Cem Concr Res 2008;38(3):275–89.
[11] Hinrichs W, Odler I. Investigation on the hydration of Portland blast furnace slag cement. Adv Cem Res 1989;2(5):9–20.
[12] Harrisson AM, Winter NB, Taylor HWF. Microstructure and microchemistry of slag cement pastes. MRS Proc 1986;86:213–22.
[13] Taylor HFW. Cement chemistry. 2nd ed. London: Thomas Telford; 1997.
[14] Bentz DP. A three-dimensional cement hydration and microstructural program. I. Hydration rate, heat of hydration and chemical shrinkage. NISTIR 5756; 1995. <http://ciks.cbt.nist.gov/bentz/nistir5756/node15.html>.
[15] Berry EE, et al. Beneficiated fly ash: hydration microstructure and strength development in Portland cement systems. ACI SP-114; 1989: 241–73.
[16] Li W, Roy DM. Investigation of relations between porosity, pore structure and C1-diffusion of fly ash and blended cement paste. Cem Concr Res 1986;16(5):749–59.
[17] Zhou J, Ye G, Van Breugel K. Hydration process and pore structure of Portland cement paste blended with blast furnace slag. In: Tongbo S, Rongxi S, Wensheng Z, editors. Cement and concrete, contributing to global sustainability. Beijing: Foreign Languages Press; 2006. p. 417–24.
[18] Vandamme M. The nanogranular origin of concrete creep: a nanoindentation investigation of microstructure and fundamental properties of calcium-silicate-hydrates. PhD thesis. Cambridge (MA): Massachusetts Institute of Technology; 2008.
[19] Sakulich A, Li V. Nanoscale characterization of engineered cementitious composites (ECC). Cem Concr Res 2011;41(2):169–75.
[20] Biolzi L, Cattaneo S, Rosati G. Evaluating residual properties of thermally damaged concrete. Cem Concr Compos 2008;30(10):907–16.
[21] Lea FM. The chemistry of cement and concrete. London: Edward Arnold Ltd.; 1983.
[22] Bazant ZP, Kaplan MP. Concrete in high temperatures, material properties and mathematical models. London: Longman Group Ltd.; 1996.
[23] Ulm FJ, Coussy O, Bazant Z. The chunnel fire. I. Chemoplastic softening in rapidly heated concrete. ASCE J Eng Mech 1999;125(3):272–82.
[24] Arioz O. Effects of elevated temperatures on properties of concrete. Fire Safety J 2007;42(8):516–22.
[25] Noumowe A, Siddique R, Rance G. Thermo-mechanical characteristics of concrete at elevated temperatures up to 310 °C. Nucl Eng Des 2009;239(3):470–6.
[26] Farage MCR, Sercombe J, Galle C. Rehydration of microstructure of cement paste after heating at temperatures up to 300 °C. Cem Concr Res 2003;33(7):1047–56.
[27] Masse S, Vetter G, Boch P, Haehnel C. Elastic modulus changes in cementitious materials submitted to thermal treatments up to 1000 °C. Adv Cem Res 2002;14(4):169–77.
[28] Guise SE. Petrographic and color analysis for assessment of fire damaged concrete. In: Jany L, et al., editors. Proceedings of the 19th international conference on cement, microscopy; 1999. p. 365–72.
[29] Powers-Couche L. Fire damaged concrete-up close. Concr Rep Dig 1992:241–8.
[30] Gustafero AH. Experiences from evaluating fire-damaged concrete structures—fire safety of concrete structures. ACI SP-80; 1983.
[31] Handoo SK, Agarwal S, Agarwal SK. Physicochemical, mineralogical, and morphological characteristics of concrete exposed to elevated temperatures. Cem Concr Res 2002;32(7):1009–18.
[32] Hertz KD. Danish investigations on silica fume concretes at elevated temperatures. ACI Mater J 1992;89(4):345–7.
[33] Poon C, Azhar S, Anson M, Wong Y. Comparison of the strength and durability performance of normal and high strength pozzolanic concretes at elevated temperatures. Cem Concr Res 2001;31(9):1291–300.
[34] Balendran RV, Rana TM, Magsood T, Tang WC. Strength and durability performance of HPC incorporating pozzolans in elevated temperatures. Struct Surv 2002;20(4):123–8.
[35] Poon C, Azhar S, Anson M, Wong Y. Performance of metakaolin concrete at elevated temperatures. Cem Concr Compos 2003;25(1):83–9.
[36] Sullivan PJE, Shansar R. Performance of concrete at elevated temperature (as measured by the reduction in compressive strength). Fire Technol 1992;28(3):240–50.
[37] Al-Akhras N, Al-Akhlas KM, Attom MF. Performance of olive waste ash concrete exposed to elevated temperatures. Fire Safety J 2009;44(3):370–5.
[38] Siddique R, Kaur D. Properties of concrete containing ground granulated blast furnace slag (GGBFS) at elevated temperatures. J Adv Res 2012;3(1):45–51.
[39] Dias WP, Khoury GA, Sullivan PJ. Mechanical properties of hardened cement paste exposed to temperatures up to 700 °C (1292 °F). ACI Mater J 1990;87(2):160–5.
[40] Chan YN, Peng GF, Anson M. Residual strength and pore structure of high-strength concrete and normal-strength concrete after exposure to high temperatures. Cem Concr Compos 1999;21(1):23–7.
[41] Ghosh S, Nasser KW. Effects of high temperature and pressure on strength and elasticity of lignite fly ash and silica fume concrete. ACI Mater J 1996;93(1):51–60.
[42] Hossain KMA. High strength blended cement concrete incorporating volcanic ash: performance at high temperature. Cem Concr Compos 2006;28(6):535–45.
[43] Nasser KW, Marzouk HM. Properties of mass concrete containing fly ash at high temperatures. ACI Mater J 1979;76(4):537–51.
[44] Wang XS, Wu BS, Wang QY. Online SEM investigation of microcrack characteristics of concretes at various temperatures. Cem Concr Res 2004;35(7):1385–90.
[45] McCoy BC. Enhanced sustainability concrete mixtures: effects of elevated temperature exposure on changes in microstructure and elastic properties and the development of modified layered-sectional analysis for forensic investigation. MSc thesis. Raleigh (NC): North Carolina State University; 2011.
[46] Miller M, Bobko C, Vandamme M, Ulm FJ. Surface roughness criteria for cement paste nanoindentation. Cem Concr Res 2008;38(4):467–76.
[47] Trtik P, Münch B, Lura P. A critical examination of statistical nanoindentation on model materials and hardened cement pastes based on virtual experiments. Cem Concr Compos 2009;3(10):705–14.
[48] Lura P, Trtik P, Münch B. Validity of recent approaches for statistical nanoindentation of cement pastes. Cem Concr Compos 2011;33(4):457–65.
[49] Ulm FJ, Vandamme M, Jennings HM, Vanzo J, Bentivegna M, Krakowiak KJ, et al. Does microstructure matter for statistical nanoindentation techniques? Cem Concr Compos 2010;32(1):92–9.
[50] Oliver WC, Pharr GM. Measurement of hardness and elastic modulus by instrumented indentation: advances in understanding and refinements to methodology. J Mater Res 2004;19(1):3–20.
[51] Krakowiak KJ, Lorenco PB, Ortega JA, Ulm FJ. Multitechnique investigation of extruded clay brick microstructure. J Am Ceram Soc 2011;94(9):3012–22.
[52] Mclachlan GJ, Peel D, Basford KE, Adams P. The EMMIX software for the fitting of mixtures of normal and t-components. J Stat Soft 1999;4(2):1–15.
[53] Mclachlan GJ, Peel D. Finite mixture models. Hoboken (NJ): Wiley-Interscience; 2000.